THE JOURNAL OF PHYSICAL CHEMISTRY LETTERS
A JOURNAL OF THE AMERICAN CHEMICAL SOCIETY

pubs.acs.org/JPCL

Letter

Simultaneous Passivation of Perovskite Interfaces at Multiple Active Sites Improves Device Performance: Combining Theory and Experiment

Li Liu,* Huan Bi,* Yongheng Chen, Xifang Chen, Pengyu Su, Gongfa Li, Hanjun Zou, and Zao Yi*

Cite This: *J. Phys. Chem. Lett.* 2024, 15, 766−772

Read Online

ACCESS | Metrics & More | Article Recommendations | Supporting Information

ABSTRACT: A multisite interface passivation material named 2-mercapto-4-methyl-5-thiazoleacetic acid (MMTA) is used to optimize the perovskite film top interface. DFT calculations and experiments show that MMTA can effectively passivate interface defects. Finally, the champion device's photoelectric conversion efficiency reached 23.44%, which possessed long-term stability

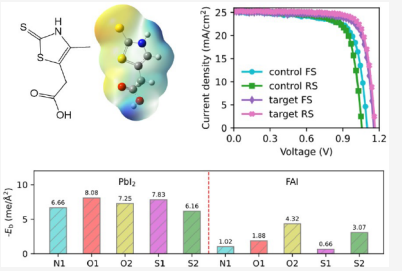

Over the past decade, organometallic halide perovskite materials have found extensive applications in solar cells, light-emitting diodes, and memory devices. This popularity is attributed to their remarkable attributes, including an excellent light absorption coefficient, long carrier diffusion length, and high tolerance to defects.[1,2] Among them, single-cell perovskite solar cells (PSCs) certified photoelectric conversion efficiency (PCE) has reached 26.1%, which is regarded as the mainstay of the third-generation photovoltaic market.[3] However, weak interface contacts and numerous film defects result in a poor efficiency. Therefore, interface engineering is essential for optimizing devices.

Various molecules have been explored in the broader field of PSCs to passivate and repair interface defects.[4−6] These include Lewis acids, Lewis bases, salts, 2D perovskites, quantum dots (QDs), and more.[7−9] The Lewis base molecule has been proven effective in passivating interfacial defects through coordination interactions with undercoordinated Pb^{2+} (halide vacancies) defects at the interface. Our previous work has also proven that modifying perovskite films can improve device efficiency and stability.[10,11] Nevertheless, the majority of passivating molecules feature only a single active site (N, O, or S electron donor) capable of interacting with uncoordinated Pb^{2+}. Even molecules with multiple active sites, such as polymers,[12] face challenges simultaneously passivating defects due to steric hindrance. To fully harness the capabilities of Lewis base defect passivation, it is crucial to develop and fine-tune multiactive-site passivating molecules that effectively reduce interfacial nonradiative recombination losses.

Here, 2-mercapto-4-methyl-5-thiazoleacetic acid (MMTA) is employed as a multisite interface modification molecule to modify the top interface of perovskite. Experimental results show that through introducing MMTA, the quality of the perovskite film is improved. Meanwhile, the enhanced interface connection significantly reduces the nonradiative recombination at the interface and improves the transport of interface carriers. Moreover, the density-functional theory (DFT) results further proved the multisite advantages of MMTA. Finally, the PCE based on MMTA modification reached 23.44% and demonstrated excellent stability. This work guides the rational design of multiple sites to passivate film defects and optimize device performance.

The device structure employed in this study is listed in Figure 1a. MMTA was introduced into the top interface of the perovskite film. Figure 1b shows the electrostatic potential diagram (ESP) of the MMTA. Rich electronegativities in MMTA are expected to combine with the cationic defects (e.g., undercoordinated Pb or halide vacancies) and further improve the film quality. X-ray photoelectron spectroscopy (XPS) was used to explore the chemical interactions between MMTA and perovskite film.[13] As shown in Figure 1c, the Pb $4f_{7/2}$ and Pb $4f_{5/2}$ of the perovskite film shift toward higher binding energy while MMTA modified, which suggests that there is indeed a strong chemical interaction between MMTA and perovskite. Interestingly, the Pb^0 XPS signal disappears while the perovskite film was modified with MMTA, indicating that MMTA could effectively interact with the undercoordinated Pb^{2+} and reduce defects in the perovskite film.

Received: November 29, 2023
Revised: January 6, 2024
Accepted: January 9, 2024
Published: January 16, 2024

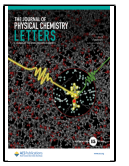

https://doi.org/10.1021/acs.jpclett.3c03352
J. Phys. Chem. Lett. 2024, 15, 766−772

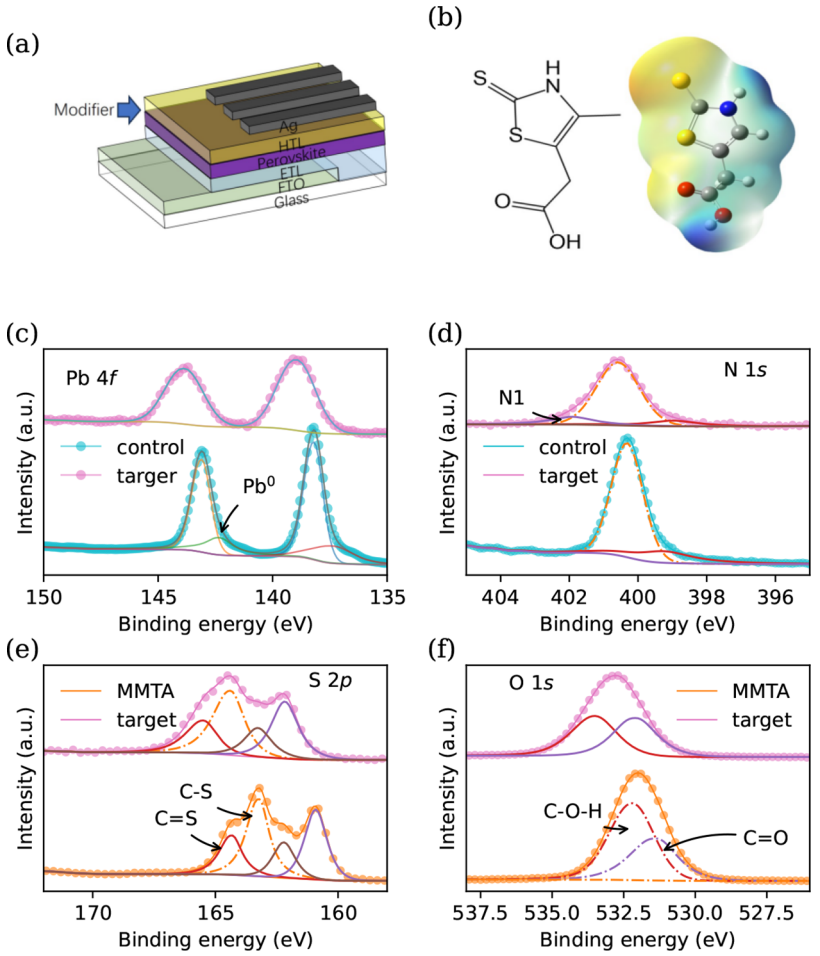

Figure 1. (a) The device structure employed in this study. (b) ESP and the molecular formula of the MMTA. Perovskite film XPS spectra of (c) Pb 4f and (d) N 1s without (control) or with (target) MMTA modification. (e) S 2p and (f) O 1s XPS spectra of the perovskite films with MMTA modification and pure MMTA powder.

Further study was carried out to understand the multisite in the MMTA (Figure S1). Figure 1d shows the N 1s of the control and target film. For target film, the 402.01 eV peaks are designated as N−H vibrations. In addition, a significant peak shift while perovskite film modified with MMTA suggests that N in the MMTA can generate a coordination bond with undercoordinated Pb^{2+}.[14] As illustrated by S 2p spectra in Figure 1e, MMTA powder possesses two obvious peaks belonging to the vibration of the C−S and C═S.[15] The peaks of the C−S and C═S in the target film shift toward high binding energy after MMTA modification. This result indicates a strong chemistry between S in MMTA and undercoordinated Pb^{2+} in the perovskite. The XPS O 1s spectra in Figure 1f illustrate that the O 1s spectrum of the modified sample can be deconvoluted into two peaks at 532.76 and 533.51 eV, corresponding to C═O and C−O−H, respectively. The binding energy of C═O shifted from 531.35 to 532.76 eV after MMTA modification serves as confirmation of the interaction between C═O in MMTA and undercoordinated Pb^{2+}. This coordination bond is established, as the oxygen in C═O of the MMTA provides a lone electron pair to undercoordinated Pb^{2+}. Additionally, the peak position of O 1s in C−O−H in MMTA shifts when deposited on a perovskite film, indicating a chemical interaction between O in C−O−H and undercoordinated Pb^{2+}. In summary, the XPS results suggest that multiple active sites in MMTA can chemically interact with undercoordinated Pb^{2+} in the perovskite.

In addition, we conducted DFT calculations to investigate the interface structures and binding energies on the atomic level. Here, we selected a simple perovskite model (the (001) surface of $FAPbI_3$) to uncover the unknown interaction between MMTA and perovskite. We conducted a systematic study on two typical of interfaces involving $FAPbI_3$ perovskite adsorbing MMTA ligands. These interfaces encompassed the inorganic PbI_2 and organic FAI planes in contact with the MMTA ligands. The optimized ground-state structures are shown in Figure S2a−h. The PbI_2 and FAI planes exhibit distinct active sites, including iodine atom vacancy, iodine dangling bonds, bare FA cations, etc. We use differential charge density further to visualize the strong chemical interaction between MMTA and perovskite. As shown in Figure 2a−e, while different active sites contact the PbI_2 surface, obvious charge transfer occurs, which means that different active sites can form a strong chemical interaction with the PbI_2 surface. This chemical interaction can effectively passivate possible defects in the film. In addition, the charge transfer between FAI and MMTA was also evaluated, and an obvious charge transfer can be observed, as shown in Figure 2f−j. The differential charge density visually shows the direct strong chemical interaction between the different interfaces of MMTA and perovskite, consistent with the XPS results.

https://doi.org/10.1021/acs.jpclett.3c03352
J. Phys. Chem. Lett. 2024, 15, 766−772

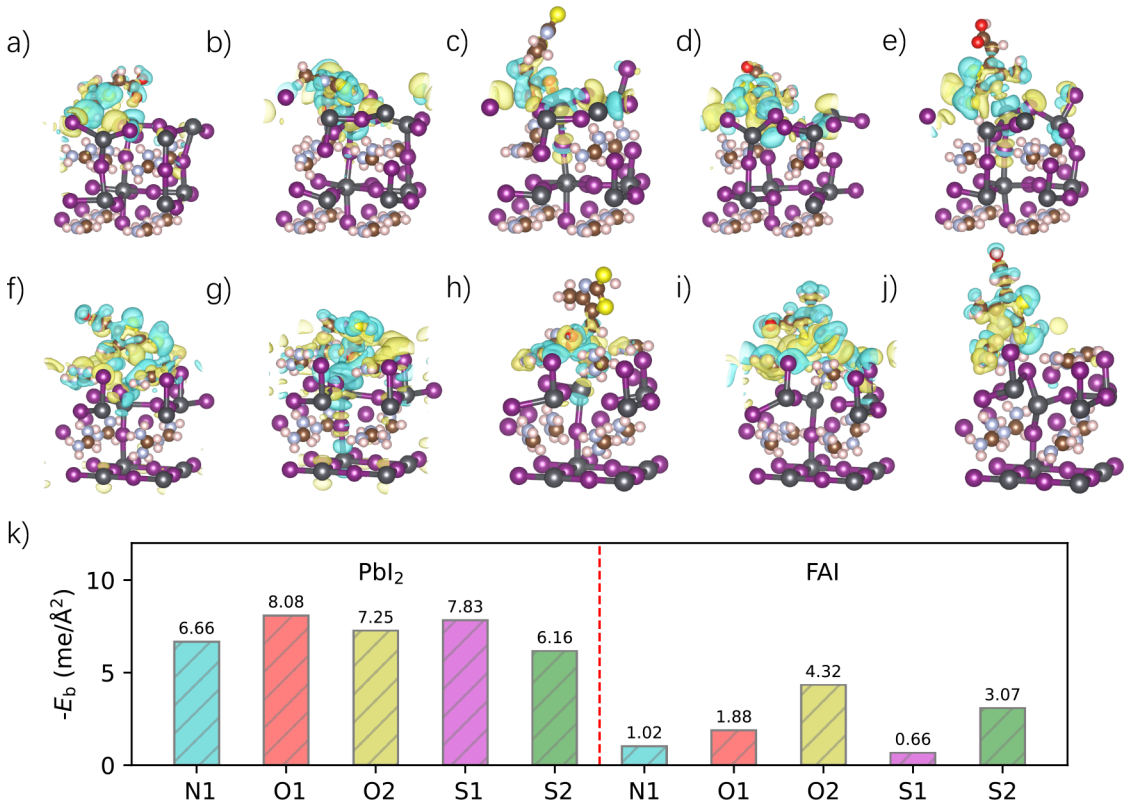

Figure 2. Interfaces for the inorganic PbI_2 plane and FAI plane with the iodine defect in contact with the different sites of MMTA. PbI_2 interface with (a) N1, (b) O1, (c) O2, (d) S1, and (e) S2 of MMTA. FAI interface with (f) N1, (g) O1, (h) O2, (i) S1, and (j) S2 of MMTA. (i) Binding energies of these interfaces.

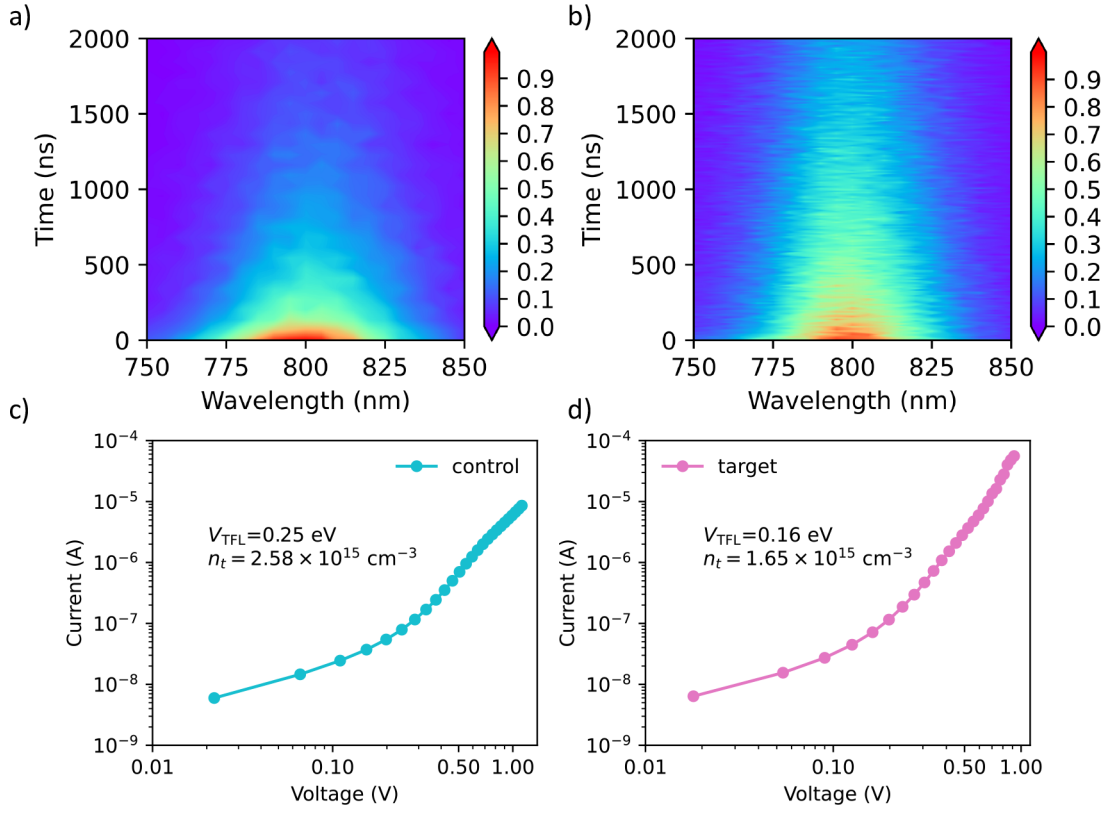

Figure 3. T-TRPL of the perovskite film (a) without or (b) with MMTA modification deposited on glass. Dark $I-V$ curves of the device with the structures of (c) FTO/PTAA/perovskite/Spiro-OMeTAD/Ag and (d) FTO/PTAA/perovskite/MMTA/Spiro-OMeTAD/Ag.

https://doi.org/10.1021/acs.jpclett.3c03352
J. Phys. Chem. Lett. 2024, 15, 766−772

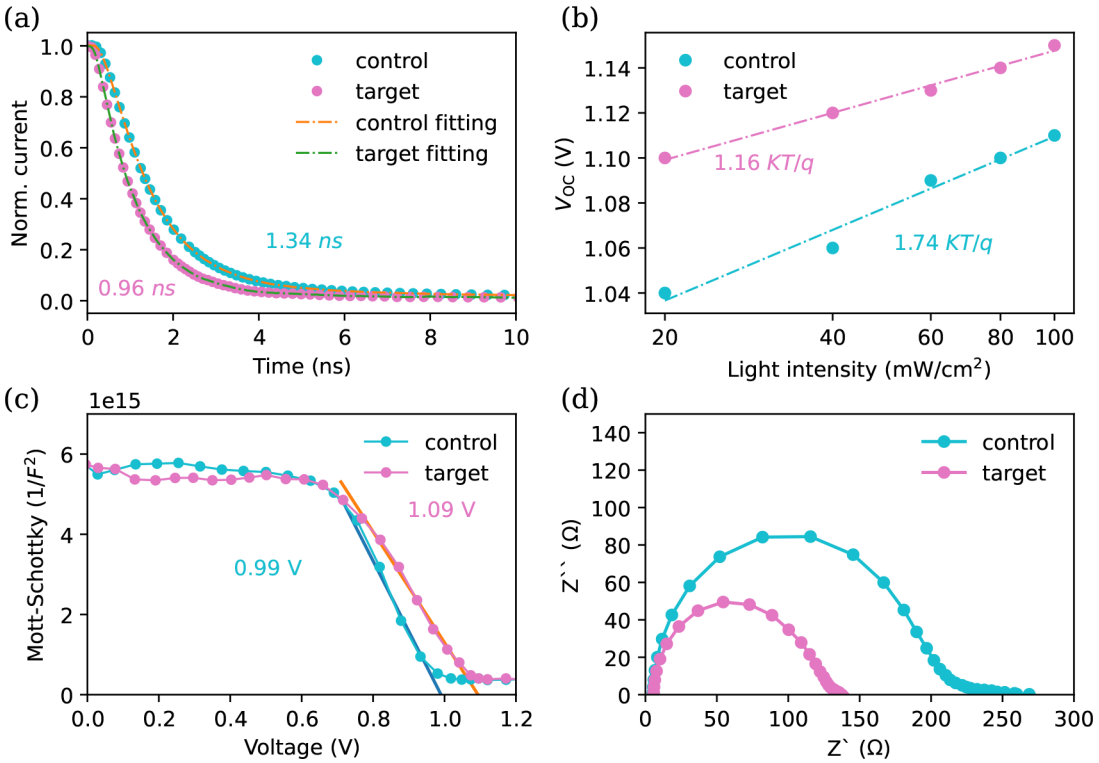

Figure 4. (a) Transient photocurrent decay curves of the control and target devices. (b) V_{OC} vs light intensity for the control and target devices. (c) Mott−Schottky curves of the control and target devices. The voltage intercept of the $1/F^2$ curves determined V_{bi}. (d) The control and target device's Nyquist plots were measured at a bias of 0.5 V under dark conditions.

Furthermore, we calculated the binding energy (E_b) of the MMTA and perovskite's structure to evaluate the total structure stability and the different chemical interactions with different structures of the MMTA with perovskite. Different sites on MMTA are named N1, O1, O2, S1, and S2 (Figure S3). As shown in Figure 2k, various E_b values for the different configurations are exhibited. The binding energies of $FAPbI_3$ with the PbI_2 planes adsorbing MMTA ligands are considerably higher than those with the FAI plane. Moreover, the adsorption of multiple active sites of MMTA ligands exhibits the maximum binding energy, indicating that this multiactive-site adsorption style is the most thermodynamically favorable. Among all the single-active-site adsorption configurations, PbI_2-MMTA_O1 demonstrates the highest E_b of 8.08 meV/Å^2, signifying that the C═O group has the strongest chemical interaction with undercoordinated Pb^{2+}. As previously discussed, our experimental findings have confirmed that the multiple active sites (including N1, O1, O2, S1, and S2) in the MMTA ligand can indeed chemically interact with perovskite films, specifically undercoordinated Pb^{2+}, as supported by XPS.

The robust chemical interaction observed prompted us to further investigate the impact of MMTA on the quality of the perovskite film. Time-dependent time-resolved photoluminescence (T-TRPL) with the structure of glass/perovskite and glass/perovskite/MMTA was tested and presented in Figure 3a and b, respectively. For the control film, the obvious fluorescence lifetime appears between 775 and 825 nm, and the longest lifetime occurs at 800 nm and shows the tail to 1000 ns. For the target film, the obvious fluorescence lifetime appears between 783 and 816 nm, and the longest lifetime occurs at 797 nm and shows a tail of 2000 ns. A longer tail means that the perovskite film modified with MMTA has a longer carrier lifetime. Meanwhile, the target film shows a narrower half-width PL peak and lower PL wavelength obtained by T-TRPL. Here, we fitted the TRPL curve at 800 nm; the results are shown in Figure S4. The target perovskite film exhibits a longer carrier lifetime of 1818.55 ns, while the control film is only 1384.46 ns. These results indicate that the MMTA interface modification can passivate surface defects of perovskite films and improve the quality of the film. Furthermore, space charge limited current (SCLC) measurements were conducted to assess the defect densities within the perovskite films quantitatively. The typical current−voltage (I−V) curves obtained in the absence of light are presented in Figure 3c and d. The defect density was quantified using the following equation:[16−18]

$$n_t = \frac{2\varepsilon\varepsilon_0 V_{TFL}}{eL^2} \quad (1)$$

where ε_0 represents the vacuum dielectric constant, ε is the dielectric constant of the perovskite, V_{TFL} corresponds to the trap-filled limit voltage, e denotes the elementary charge, and L represents the thickness of the perovskite film.[16,17] The defect density in the control perovskite film is 2.58 × 10^{15} cm^{-3}, higher than the 1.65 × 10^{15} cm^{-3} observed in the target perovskite film. T-TRPL and SCLC results collectively indicate that MMTA effectively reduces the defects of the perovskite films and improves the quality of the perovskite film.

As reported, improved film quality can reduce nonradiative recombination of the device.[19] Transient photocurrent (TPC) measurement was employed to investigate the charge transfer. As presented in Figure 4a, the carrier lifetime of the control device is 1.34 ns while the target is 0.96 ns, suggesting that the

https://doi.org/10.1021/acs.jpclett.3c03352
J. Phys. Chem. Lett. 2024, 15, 766−772

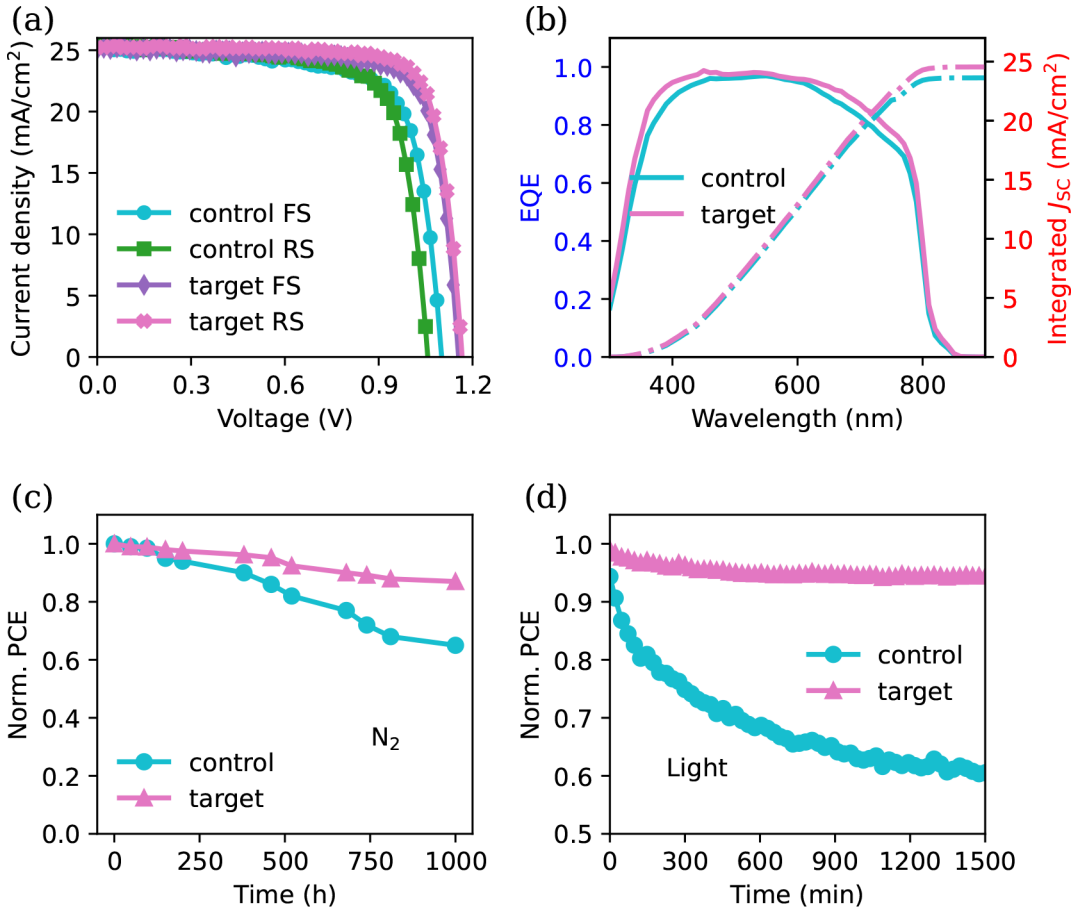

Figure 5. (a) $J-V$ curves and (b) EQE spectra of the champion control and target devices. (c) N_2 and (d) light stability of unpackaged devices stored in N_2-filled glovebox.

interfacial charge transfer improved after MMTA modification. Furthermore, the device's nonradiative recombination were evaluated via the built-in potential (V_{bi}) and ideality factor (m).[20,21] As shown in Figure 4b, the target device exhibits a lower m of 1.16 than the control device (m = 1.74), showing that the surface nonradiative recombination is significantly decreased by MMTA modification. Then, Mott−Schottky curves were measured to calculate V_{bi}, as shown in Figure 4c. The V_{bi} of the target device is 1.09 V, while the control is only 0.99 V, proving the improved interfacial charge extraction. Transient photovoltage (TPV) results show that the carrier lifetime of the control device is 9.17 ns while the target is 10.48 ns, indicating that the MMTA can indeed reduce the nonradiative recombination of the device (Figure S5). Additionally, electrochemical impedance spectroscopy (EIS) was employed to explore the effect of MMTA passivation on interfacial charge transfer and recombination. Figure 4d exhibits the Nyquist plots of the control and target devices obtained at a bias of 0.5 V. The series resistance (R_s) and recombination resistance (R_{rec}) in parallel with a chemical capacitance (C_μ) were extracted from the EIS spectra (the fitting model is exhibited in Figure S6). Compared with the control device, there is an apparent R_s decrease and R_{rec} increase of the MMTA modification device. This result suggests that the MMTA can effectively reduce nonradiative recombination and accelerate carrier transmission, further improving the PSCs' FF and V_{OC}.

Increased charge transfer, improved film quality, and reduced nonradiative recombination encouraged us to investigate the effect of MMTA modification on PSC performance. The photovoltaic parameters of the PSCs with different concentrations of MMTA modifications are compared and displayed in Figure S7. Compared with the control device, all photovoltaic parameters of the PSCs with 0.5 mg/mL MMTA modification are improved. Given that the control and target perovskite films exhibit nearly identical absorption intensities (Figure S8), the enhanced interfacial charge transfer is presumed to be the primary factor responsible for the increased J_{SC}. Furthermore, the suppressed interfacial nonradiative recombination is expected to significantly contribute to the improved V_{OC} and FF. Figure 5a shows the $J-V$ curves of the best device with or without MMTA modification. The champion target device delivered a J_{SC} of 24.94 mA/cm^2 and 25.22 mA/cm^2, a V_{OC} of 1.155 and 1.165 V, an FF of 0.792 and 0.798, and a PCE of 22.81% and 23.44% in FS and RS, respectively. In contrast, the control device achieved a J_{SC} of 24.82 mA/cm^2 and 25.14 mA/cm^2, a V_{OC} of 1.059 and 1.101 V, an FF of 0.761 and 0.765, and a PCE of 20.00% and 21.17%, in FS and RS, respectively. External quantum efficiency (EQE) spectra were tested to prove the current density of the device further, as shown in Figure 5b; the current density of the device modified by MMTA is 24.67 mA/cm^2 while that of the control device is 24.02 mA/cm^2, consisting of the $J-V$ curves.

In addition, we conducted an extensive assessment of the effect of MMTA treatment on N_2 and light stability of

https://doi.org/10.1021/acs.jpclett.3c03352
J. Phys. Chem. Lett. 2024, 15, 766−772

perovskite solar devices. We placed unpackaged devices in a glovebox filled with N_2. After 1000 h of aging, the target device maintained 87% of its original efficiency, while the control maintained only 65%, as shown in Figure 5c. Additionally, the unencapsulated device was placed under light for continuous aging. After 1500 min, the control device degraded to 60.5% of the original efficiency, while the target was retained at 97% (Figure 5d). Such significant stability improvement can be attributed to the improved film quality and reduced nonradiative recombination in the device. This result highlights that employing a multiactive-site interfacial engineering strategy can enhance both efficiency and long-term operational durability.

In summary, we have introduced a novel strategy for passivating interface defects in MA-free perovskite films through a multiactive site Lewis base molecule (MMTA). Our combined experimental and theoretical findings demonstrate that the multiple active sites in MMTA molecules can chemically interact with undercoordinated Pb^{2+} defects on the perovskite film's surface. Moreover, DFT results suggest that multiactive site adsorption is thermodynamically more favorable than single-active site adsorption, maximizing the defect passivation effect of MMTA. The modification with MMTA enhances film quality and reduces nonradiative recombination within the device. Consequently, the PCE of the MMTA-modified device increases from 21.17% to 23.44% compared to the reference. This work underscores the significance of utilizing multiactive site molecules for passivating interface defects. We firmly believe that reducing nonradiative recombination losses on the surface of perovskite films, achieved by developing innovative multiactive site defect passivation molecules, is essential to achieving the efficiency and stability required for commercialization.

■ ASSOCIATED CONTENT

Supporting Information

The Supporting Information is available free of charge at https://pubs.acs.org/doi/10.1021/acs.jpclett.3c03352.

Details of materials and methods and additional data on material and device characterizations (PDF)

■ AUTHOR INFORMATION

Corresponding Authors

Li Liu − *Joint Laboratory for Extreme Conditions Matter Properties, School of Mathematics and Physics, Southwest University of Science and Technology, Mianyang, People's Republic of China 621010*; Email: liuli_phy@swust.edu.cn

Huan Bi − *Graduate School of Informatics and Engineering, The University of Electro-Communications, Tokyo, Japan 182-8585*; orcid.org/0000-0001-7680-9816; Email: hbi.trans.sci@gmail.com

Zao Yi − *Joint Laboratory for Extreme Conditions Matter Properties, School of Mathematics and Physics, Southwest University of Science and Technology, Mianyang, People's Republic of China 621010*; orcid.org/0000-0002-7019-7481; Email: yizaomy@swust.edu.cn

Authors

Yongheng Chen − *Joint Laboratory for Extreme Conditions Matter Properties, School of Mathematics and Physics, Southwest University of Science and Technology, Mianyang, People's Republic of China 621010*

Xifang Chen − *Joint Laboratory for Extreme Conditions Matter Properties, School of Mathematics and Physics, Southwest University of Science and Technology, Mianyang, People's Republic of China 621010*; orcid.org/0000-0003-4528-5508

Pengyu Su − *School of Electronic Information Engineering, Yangtze Normal University, Chongqing, People's Republic of China 408100*

Gongfa Li − *Hubei Key Laboratory of Mechanical Transmission and Manufacturing Engineering, Wuhan University of Science and Technology, Wuhan, People's Republic of China 430081*

Hanjun Zou − *Analytical and Testing Center, Chongqing University, Chongqing, P. R. China 401331*

Complete contact information is available at: https://pubs.acs.org/10.1021/acs.jpclett.3c03352

Notes

The authors declare no competing financial interest.

■ ACKNOWLEDGMENTS

The project is supported by the Open Fund of Hubei Key Laboratory of Mechanical Transmission and Manufacturing Engineering at Wuhan University of Science and Technology (MTMEOF2021B02), the Doctoral Fund of Southwest University of Science and Technology (no. 21zx7111). The authors would like to acknowledge Prof. Qing Shen (The University of Electro-Communications) for a valuable discussion.

■ REFERENCES

(1) Bi, H.; Liu, J.; Zhang, Z.; Wang, L.; Beresneviciute, R.; Tavgeniene, D.; Kapil, G.; Ding, C.; Baranwal, A. K.; Sahamir, S. R.; Sanehira, Y.; Segawa, H.; Grigalevicius, S.; Shen, Q.; Hayase, S. All-Perovskite Tandem Solar Cells Approach 26.5% Efficiency by Employing Wide Bandgap Lead Perovskite Solar Cells with New Monomolecular Hole Transport Layer. *ACS Energy Lett.* **2023**, *8*, 3852−3859.

(2) Veldhuis, S. A.; Boix, P. P.; Yantara, N.; Li, M.; Sum, T. C.; Mathews, N.; Mhaisalkar, S. G. Perovskite Materials for Light-Emitting Diodes and Lasers. *Adv. Mater.* **2016**, *28*, 6804−34.

(3) Bi, H.; Liu, J.; Zhang, Z.; Wang, L.; Kapil, G.; Wei, Y.; Kumar Baranwal, A.; Razey Sahamir, S.; Sanehira, Y.; Wang, D.; Yang, Y.; Kitamura, T.; Beresneviciute, R.; Grigalevicius, S.; Shen, Q.; Hayase, S. Ferrocene Derivatives for Improving the Efficiency and Stability of MA-Free Perovskite Solar Cells from the Perspective of Inhibiting Ion Migration and Releasing Film Stress. *Adv. Sci.* **2023**, *10*, 2304790.

(4) Isikgor, F. H.; Zhumagali, S.; T. Merino, L. V.; De Bastiani, M.; McCulloch, I.; De Wolf, S. Molecular Engineering of Contact Interfaces for High-performance Perovskite Solar Cells. *Nat. Rev. Mater.* **2023**, *8*, 89−108.

(5) Jiang, Q.; et al. Surface Reaction for Efficient and Stable Inverted Perovskite Solar Cells. *Nature* **2022**, *611*, 278−283.

(6) Li, Z.; Li, B.; Wu, X.; Sheppard, S. A.; Zhang, S.; Gao, D.; Long, N. J.; Zhu, Z. Organometallic-functionalized Interfaces for Highly Efficient Inverted Perovskite Solar Cells. *Science* **2022**, *376*, 416−420.

(7) Fan, Y.; Wang, X.; Miao, Y.; Zhao, Y. The Chemical Design in High-Performance Lead Halide Perovskite: Additive vs Dopant? *J. Phys. Chem. Lett.* **2021**, *12*, 11636−11644.

(8) Wang, Y.; Liu, T.; Zhang, J.; Liu, H.; Li, H.; Lv, Y.; Guo, X.; Liu, X.; Tu, L.; Chang, Y.; Li, B. A 2D/3D Heterojunction Engineered for Carbon-Based Hole-Transport-Layer-Free Perovskite Solar Cells. *Sustain. Energy Fuels* **2023**, *7*, 2853−2860.

(9) Liu, T.; Su, P.; Liu, L.; Wang, J.; Feng, S.; Zhang, J.; Xu, R.; Yang, H.; Fu, W. An Ionic Compensation Strategy for High-

Performance Mesoporous Perovskite Solar Cells: Healing Defects with Tri-Iodide Ions in A Solvent Vapor Annealing Process. *J. Mater. Chem. A* **2019**, *7*, 353−362.
(10) Bi, H.; et al. Efficiency Enhancement of Wide Bandgap Lead Perovskite Solar Cells with PTAA Surface-Passivated with Monomolecular Layer from the Viewpoint of PTAA Band Bending. *ACS Appl. Mater. Interfaces* **2023**, *15*, 41549−41559.
(11) Su, P.; Bi, H.; Ran, D.; Liu, L.; Hou, W.; Wang, G.; Shi, W. Multifunctional and Multi-site Interfacial Buffer Layer for Efficient and Stable Perovskite Solar Cells. *Chem. Eng. J.* **2023**, *472*, 145077.
(12) Gao, F.; Zhao, Q. Facet Engineering: A Promising Pathway toward Highly Efficient and Stable Perovskite Photovoltaics. *J. Phys. Chem. Lett.* **2023**, *14*, 4409−4418.
(13) Liu, T.; Scheidt, R. A.; Zheng, X.; Joy, S.; Jiang, Q.; Atapattu, H. R.; Chen, M.; Pruett, H.; Zhu, K.; Luther, J. M.; Beard, M. C.; Graham, K. R. Tuning Interfacial Energetics with Surface Ligands to Enhance Perovskite Solar Cell Performance. *Cell Rep. Phys. Sci.* **2023**, *4*, 101650.
(14) Laskar, M. A. R.; Luo, W.; Ghimire, N.; Chowdhury, A. H.; Bahrami, B.; Gurung, A.; Reza, K. M.; Pathak, R.; Bobba, R. S.; Lamsal, B. S.; Chen, K.; Rahman, M. T.; Rahman, S. I.; Emshadi, K.; Xu, T.; Liang, M.; Zhang, W.-H.; Qiao, Q. Phenylhydrazinium Iodide for Surface Passivation and Defects Suppression in Perovskite Solar Cells. *Adv. Funct. Mater.* **2020**, *30*, 2000778.
(15) Wang, H.; Qiu, X.; Wang, W.; Jiang, L.; Liu, H. Iron Sulfide Nanoparticles Embedded Into a Nitrogen and Sulfur Co-doped Carbon Sphere as a Highly Active Oxygen Reduction Electrocatalyst. *Front. Chem.* **2019**, *7*, 855.
(16) Ding, X.; Wang, H.; Miao, Y.; Chen, C.; Zhai, M.; Yang, C.; Wang, B.; Tian, Y.; Cheng, M. Bi(trifluoromethyl) Benzoic Acid-Assisted Shallow Defect Passivation for Perovskite Solar Cells with an Efficiency Exceeding 21%. *ACS Appl. Mater. Interfaces* **2022**, *14*, 3930−3938.
(17) Hou, W.; Guo, M.; Chang, Y.; Zhu, S.; Bi, H.; Shen, Q.; Xiao, Y.; Han, G. In Situ Lead Oxysalt Passivation Layer for Stable and Efficient Perovskite Solar Cells. *Chem. Commun.* **2022**, *58*, 12708−12711.
(18) Wang, W.; Zhou, Q.; He, D.; Liu, B.; Bai, L.; Xu, C.; Song, Q.; Zhao, P.; Chen, C.; Sun, K.; Yang, H.; Zang, Z.; Lee, D.; Chen, J. Self-Formed Multifunctional Grain Boundary Passivation Layer Achieving 22.4% Efficient and Stable Perovskite Solar Cells. *Solar RRL* **2022**, *6*, 2100893.
(19) Chen, J.; Park, N. G. Causes and Solutions of Recombination in Perovskite Solar Cells. *Adv. Mater.* **2019**, *31*, 1803019.
(20) Caprioglio, P.; Wolff, C. M.; Sandberg, O. J.; Armin, A.; Rech, B.; Albrecht, S.; Neher, D.; Stolterfoht, M. On the Origin of the Ideality Factor in Perovskite Solar Cells. *Adv. Energy Mater.* **2020**, *10*, 2000502.
(21) Sandberg, O. J.; Kurpiers, J.; Stolterfoht, M.; Neher, D.; Meredith, P.; Shoaee, S.; Armin, A. On the Question of the Need for a Built-In Potential in Perovskite Solar Cells. *Adv. Mater. Interfaces* **2020**, *7*, 2000041.

https://doi.org/10.1021/acs.jpclett.3c03352
J. Phys. Chem. Lett. 2024, 15, 766−772